ACS OMEGA

Article

http://pubs.acs.org/journal/acsodf

Nanoporous Fe-Based Alloy Prepared by Selective Dissolution: An Effective Fenton Catalyst for Water Remediation

Huiyan Zhang,[†,#] Yuping Feng,[†] Yangyang Cheng,[‡] Maria Dolors Baró,[†] Ainhoa Altube,[§] Eva García-Lecina,[§] Francisco Alcaide,[∥] Eva Pellicer,*[,†] Tao Zhang,[‡] and Jordi Sort*[,†,⊥]

[†]Departament de Física, Building Cc, Universitat Autònoma de Barcelona, Cerdanyola del Vallès, Barcelona E08193, Spain

[‡]Key Laboratory of Aerospace Materials and Performance (Ministry of Education), School of Materials Science and Engineering, Beihang University, 37 Xueyuanlu, Haidian District, Beijing 100191, China

[§]Unidad de Superficies Metálicas and [∥]Unidad de Materiales para Energía, IK4-CIDETEC, Paseo Miramón 196, Donostia-San Sebastián, Gipuzkoa E20009, Spain

[⊥]Institució Catalana de Recerca i Estudis Avançats (ICREA), Passeig Lluís Companys 23, Barcelona E08010, Spain

[#]School of Materials Science and Engineering, Anhui University of Technology, 59 Hudonglu, Huashan District, Ma'anshan 243002, China

Supporting Information

ABSTRACT: A fully nanoporous Fe-rich alloy, prepared by selective dissolution of melt-spun $Fe_{43.5}Cu_{56.5}$ ribbons, exhibits outstanding properties as a heterogeneous Fenton catalyst toward the degradation of methyl orange (MO) in aqueous solution. In addition, the ferromagnetic characteristics of this material enable its wireless manipulation toward specific locations within polluted wastewater. The influence of selective dissolution on the microstructure, sample morphology (surface and cross-section), elemental composition, and magnetic properties of the resulting nanoporous alloy is investigated. The dealloying procedure enhances the saturation magnetization and drastically increases the catalytic performance (i.e., the time required for full degradation of MO from the medium is reduced by a factor of approximately 2 by subjecting the $Fe_{43.5}Cu_{56.5}$ ribbons to prior dealloying). Remarkably, the effectiveness of this nanoporous material surpasses the results obtained by the homogeneous Fenton reaction using an equivalent concentration of Fe cations leached into the media from the nanoporous alloy. The different factors that promote the high catalytic activity are discussed. The outstanding catalytic activity, together with the simplicity of the synthetic procedure, makes this material very appealing for water remediation using advanced Fenton processes.

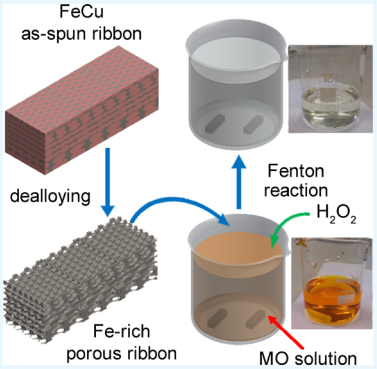

1. INTRODUCTION

With the massive growth in industrial and agricultural activities, water pollution has become one of the major environmental threats to human health and ecosystems in general.[1] Over the last few decades, various types of physical, chemical, and biological methods have been introduced to remove non-degradable organic compounds from industrial wastewater. However, most of these methods suffer from important drawbacks. For instance, physical methods, such as liquid−liquid extraction or ion-exchange, are ineffective for pollutants that are not easily adsorbable or are volatile. Membrane filtration requires very high water pressure, which in turn causes large energy power consumption. Activated carbon adsorption processes are also very costly.[2] Ozone and hypochlorite oxidation processes are efficient, but the costly equipment and secondary pollution produced by the residual chlorine make them undesirable.[3] In fact, many of these methods simply convert the pollutants to other compounds, rather than actually eliminating them.[4]

Remarkably, some advanced chemical oxidation processes can induce almost complete mineralization of a wide range of organic pollutants. For example, Fenton reactions (i.e., iron-catalyzed hydrogen peroxide) can either oxidize the contaminant materials to smaller organic molecules or transform them into water, carbon dioxide, and salts.[5−13] Besides water remediation, Fenton reactions are also of interest in biological applications because they involve the creation of free radicals by chemicals that are present in bodily fluids. Some additional advantages of Fenton reactions are their high efficiency, simplicity in destroying contaminants, and non-necessity of sophisticated equipment.[14] Moreover, the reaction takes place under ambient conditions.[15] For these reasons, homogeneous Fenton catalysts (in which Fe cations are directly dissolved in liquid media) have been widely investigated and are now considered promising for use in wastewater treatment.[16]

Received: January 12, 2017
Accepted: February 7, 2017
Published: February 23, 2017

DOI: 10.1021/acsomega.7b00043
ACS Omega 2017, 2, 653−662

As an alternative to homogeneous Fenton, some attempts have been made to develop "heterogeneous" Fenton catalysts, that is, solid materials that are immersed, but not dissolved, in the media while providing a high catalytic activity. In principle, some of the limitations encountered by a homogeneous process might be overcome by heterogeneous Fenton oxidation processes.[17,18] Namely, it has been reported that heterogeneous Fenton oxidation exhibits a lower activation free energy than that of homogeneous Fenton reactions.[19] Furthermore, during heterogeneous Fenton reactions, high amounts of surface active sites for H_2O_2 decomposition and formation of hydroxyl radicals are available, sometimes inducing a higher removal efficiency compared to a homogeneous Fenton process.[20] Heterogeneous Fenton catalysts can be prepared by incorporating Fe ions, zero-valence iron (ZVI), or Fe oxide phases (e.g., in the form on nanoparticles) into porous scaffolds that act as support materials (e.g., zeolites, nafion, clay, or activated carbon).[21−23] Nevertheless, as the host material is inactive toward the Fenton reaction, the benefit brought by the large porosity is not fully exploited. In other words, the amount of available surface area exposed to the solution (i.e., active sites at which the reactant molecules can be adsorbed) is limited to the nanoparticles. For this reason, a fully porous active material, instead of active particles embedded in a porous support, might be a suitable alternative to enhance the Fenton efficiency. In any case, mechanical integrity of the nanoporous materials is a critical issue for their use in heterogeneous catalysis experiments.

Interestingly, it has been shown that mixed iron/copper species may also promote Fenton-like processes while allowing for a less critical dependence on the pH value. Indeed, bimetallic Fe−Cu nanoparticles introduced inside different types of two-dimensional or three-dimensional porous frameworks have shown a large potential for heterogeneous Fenton catalytic activity.[24−26] Furthermore, as Fe-based materials are often ferromagnetic, precise guiding of the catalysts toward specific locations of the polluted water by means of an externally applied magnetic field and field gradients is possible, while also offering the possibility of recovering them after use for recycling purposes.[27]

Over the last few years, progress has been made toward the development of nanoporous metallic materials by means of dealloying (i.e., selective removal of the less noble element from an alloy, by either chemical or electrochemical means).[28] The process can be applied to various combinations of binary or ternary alloys, such as Ag−Au, Pt−Al, Al−Pd−Au, Ni−Mn, Ni−Pd, or Fe−Cu, among others. In particular, it has been reported that the phase-separated Fe−Cu binary alloy, with a composition around $Fe_{43}Cu_{57}$, can be selectively etched to remove Cu and render an Fe-rich metallic alloy featuring nanometer-sized pores.[29] Although detailed structural characterization of this type of material has been previously reported,[29] most of its physical and catalytic properties, as well as its potential applications, have been largely overlooked. In this study, a three-dimensional nanoporous Fe-rich alloy is prepared by dealloying $Fe_{43.5}Cu_{56.5}$ ribbons previously synthesized by rapid solidification (see Figure 1). The phase structure, morphology, elemental composition, and magnetic properties of the ribbons before and after selective dissolution are investigated in detail. The degradation performance of methyl orange (MO) during Fenton reactions using dense as-spun and nanoporous dealloyed ribbons is assessed. Remarkably, the nanoporous material outperforms the as-quenched non-dealloyed sample. The highly efficient catalytic activity and convenient processing method make this nanoporous catalyst a prospective new candidate for heterogeneous Fenton chemistry.

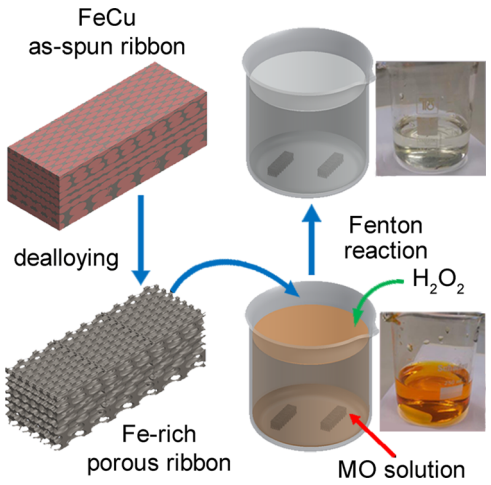

Figure 1. Schematic drawing of the dealloying process used to obtain Fe-rich nanoporous ribbons and the efficiency of the as-spun Fe−Cu and dealloyed ribbons for degradation of MO using the Fenton reaction.

2. RESULTS AND DISCUSSION

2.1. Structural and Morphological Characterization.

As shown in the X-ray diffraction (XRD) patterns of Figure 2,

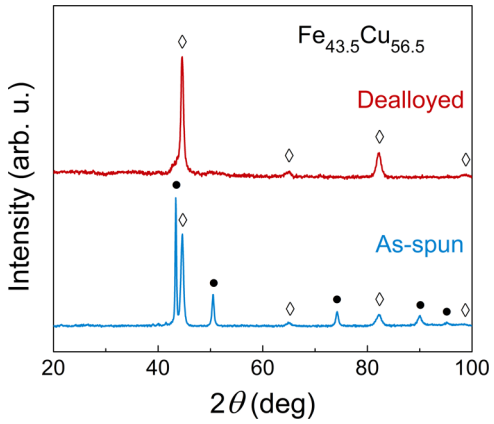

Figure 2. XRD patterns of the $Fe_{43.5}Cu_{56.5}$ alloy before and after selective dissolution in 0.1 M HNO_3 at an applied voltage of 14 V for 5 min. The peaks correspond to the fcc-Cu (black filled circle) and bcc-Fe (open diamond) phases, respectively.

typical peaks of fcc-Cu and bcc-Fe phases can be identified in the as-spun ribbon, which indicate the occurrence of phase separation. However, after selective etching, the peaks from fcc-Cu almost vanished, whereas those from bcc-Fe remained clearly visible. This demonstrates that the dealloying treatment is very effective in drastically reducing the amount of the fcc-Cu phase.

The gradient of the cooling rate across the ribbon during melt-spinning causes a variation in the surface morphology and microstructure between the free side and wheel side of the as-spun ribbon.[30] Field-emission scanning electron microscopy (FESEM) images of both sides of the ribbon, as well as its

DOI: 10.1021/acsomega.7b00043
ACS Omega 2017, 2, 653−662

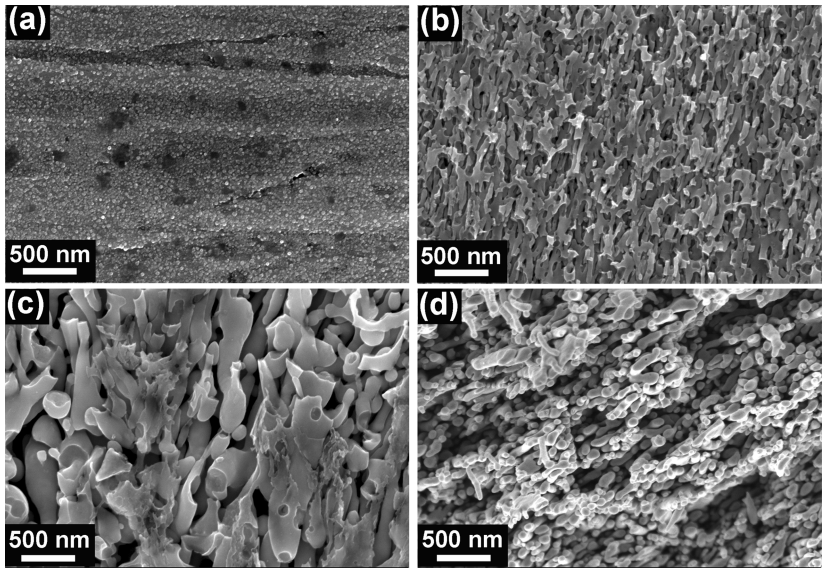

Figure 3. SEM images of (a) the polished as-spun $Fe_{43.5}Cu_{56.5}$ ribbon (taken on the wheel side) and (b–d) the dealloyed ribbon: (b) wheel side, (c) free side, and (d) fracture cross-section.

cross-section, for the as-spun and dealloyed states, are displayed in Figure 3. Compared with the rather dense appearance of the as-spun ribbon (Figure 3a), a fully porous morphology is observed after selective etching (Figure 3b). However, the pore size of the dealloyed sample varies from ∼50−100 to ∼500 nm when comparing the wheel side with the free side (cf. Figure 3b,c). To some extent, this could actually be anticipated, as the microstructure at the wheel side (faster cooling rate) is more refined than that at the air side. The ligaments are rather elongated and mostly oriented parallel to the ribbon plane, their size varying between ∼50 and ∼300 nm.

Cross-sectional analyses of the dealloyed ribbon indicated that etching and hence the occurrence of porosity were accomplished through the entire ribbon thickness (Figure 3d). A low-magnification SEM image of the cross-section is shown in Figure S1 (Supporting Information). The compositions of the ribbons, measured by energy-dispersive X-ray (EDX) analyses at different locations of the samples before and after dealloying, are listed in Table 1. Slight variations in the amounts of Fe and Cu exist between the wheel and free sides of the as-spun ribbons. Remarkably, a clear enrichment in Fe is observed in the dealloyed nanoporous ribbons, which is in agreement with the XRD results. The oxygen content also increases a bit after dealloying, although it typically remains below 20 atom %. The occurrence of O is likely attributed to the formation of Fe oxides during electrochemical polarization. However, oxide peaks could not be detected by XRD, indicating that the oxide layer is exceedingly thin in comparison to the penetration depth of the X-rays.

Table 1. Average EDX Results (Obtained by Applying a Voltage of 10 kV) from Both Sides of the Ribbons and the Cross Sections (As-Spun and Dealloyed) before and after the Fenton Reaction

material	location	chemical composition (atom %) Fe	Cu	O
polished as-spun ribbon (before Fenton)	free side	44	52	4
	wheel side	39	58	3
dealloyed ribbon (before Fenton)	free side	61	17	22
	wheel side	69	20	11
	fracture cross-section	67	18	15
as-spun ribbon after Fenton reaction	wheel side	∼2	66	31
	fracture cross-section	∼2	75	23
dealloyed ribbon after Fenton reaction	wheel side	∼3	73	24
	fracture cross-section	∼3	76	21

2.2. Magnetic Properties. Figure 4 shows the hysteresis loops of the as-spun and dealloyed ribbons, from which a soft ferromagnetic behavior is observed. The values of saturation magnetization (M_s), remanence (M_r), and coercivity (H_c) for both samples are listed in Table 2. In general, these two materials display similar magnetic properties, which stem from the bcc-Fe-rich phase.[31] However, the nanoporous (dealloyed) Fe-rich alloy possesses higher M_s, M_r, and H_c values than those of the as-spun ribbon. The increase in M_r and M_s after dealloying can be ascribed to the removal of the paramagnetic

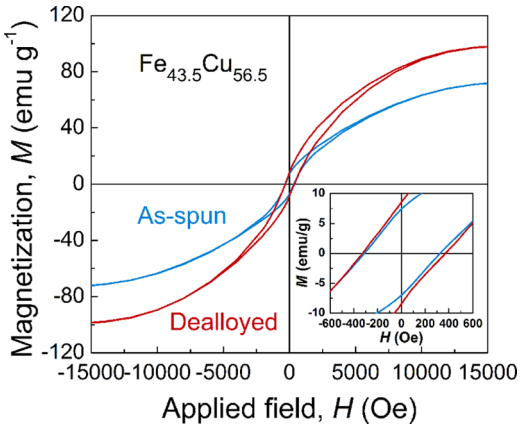

Figure 4. Hysteresis loops of $Fe_{43.5}Cu_{56.5}$ ribbons corresponding to the as-spun and dealloyed states. The inset shows a magnified view at low fields.

DOI: 10.1021/acsomega.7b00043
ACS Omega 2017, 2, 653−662

Table 2. Magnetic Properties of the As-Spun and Dealloyed Ribbons before and after the Fenton Reaction

material	saturation magnetization M_s, emu g^{-1}	remanence M_r, emu g^{-1}	coercivity H_c, Oe
polished as-spun ribbon before Fenton	73.1	7.2	317.3
dealloyed ribbon before Fenton	99.3	8.5	349.6
as-spun ribbon after Fenton reaction	~0.87	~0.06	197.5
dealloyed ribbon after Fenton reaction	~0.31	~0.03	268.8

Cu-rich phase by selective dissolution.[31,32] However, the saturation magnetization of the dealloyed ribbon is still lower than that of bulk Fe (where M_s = 218 emu g^{-1}),[33] due to the presence of Cu and O, in agreement with EDX analyses. For both samples, the values of H_c are higher than the typical ones for bulk Fe (of only a few Oe)[33] and are similar to the H_c measured in other types of Fe-based ribbons.[34] The slightly larger H_c after dealloying could be due to the hindrances for domain-wall propagation imposed by the reduced lateral dimensions of the ligaments constituting the nanoporous ribbons.

2.3. Surface Characterization. X-ray photoemission spectroscopy (XPS) characterization of the ribbons after dealloying was carried out to identify eventual changes in both the oxidation state and amounts of Fe and Cu at the surface level. The survey spectra (Figure 5) showed an increase in the Fe 2p signal and, concomitantly, a decrease in the Cu 2p peak after dealloying, in agreement with EDX analyses.

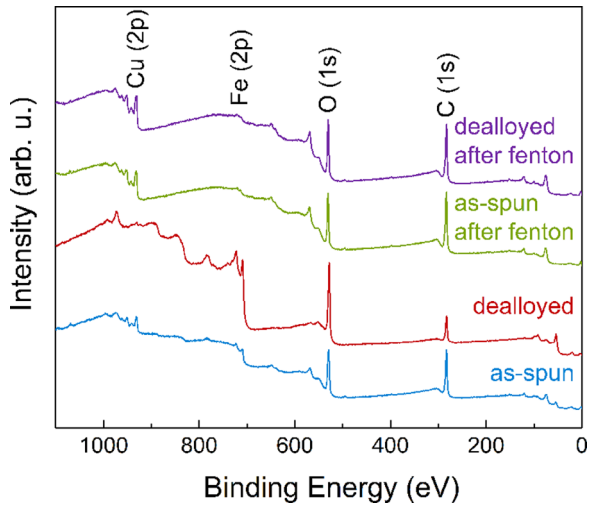

Figure 5. XPS survey spectra of the as-spun and dealloyed ribbons before and after the Fenton reaction.

Deconvoluted core-level Fe 2p spectra of the dealloyed sample are shown in Figure 6a,c. The two doublets located between 717 and 705 eV ($2p^{3/2}$) and between 730 and 720 eV ($2p^{1/2}$) indicate that iron is mostly in its oxidized state (Fe^{2+} and Fe^{3+}). Interestingly, the relative amount of Fe^{3+} in the dealloyed sample is higher than that in the as-spun one (see Figure S2a for comparison), hence indicating that the outermost surface of the dealloyed ribbon is more oxidized. The weak shoulder peak at around 706.1 eV, observed both before and after dealloying, can be ascribed to ZVI ($2p^{3/2}$). Remarkably, the ZVI signal became very strong after Ar-ion sputtering (Figure 6c), by which the outermost surface is removed.[35] Simultaneously, the contribution from oxidized Fe is strongly reduced.

The core-level Cu 2p spectra of the as-spun and dealloyed (the latter taken at the surface level and after Ar-ion sputtering) samples are shown in Figure S3. Cu mostly remains as a mixture of Cu^0, Cu^+, and Cu^{2+} in the as-spun sample. As expected, its contribution markedly reduces in the dealloyed ribbon. After Ar-ion sputtering, clear Cu peaks emerge again, in agreement with the results from Table 1; that is, Cu is not fully removed but a moderate amount (20 atom %) remains in the material. Findings from the analysis of the core-level O 1s spectra (Figure 6b,d) are in agreement with the previously observed features. Fe and Cu oxides are present at the surface of both the as-spun (Figure S2b) and dealloyed (Figure 6b) ribbons, with some differences. Namely, the relative fraction of Cu oxides is higher in the as-spun sample, in accordance with the favored removal of Cu during dealloying. After sputtering the dealloyed ribbon with Ar ions, the O signal clearly decreases (Figure 6d), which is in agreement with the detection of a large proportion of Fe and Cu in the metallic state (see Figures 6c and S3).

The results gleaned from XPS analyses of the ribbons can be summarized as follows: after dealloying, the surface is mainly covered by iron oxide precipitates, as the Cu-rich phase is removed by selective dissolution; underneath, the amount of oxides is lowered and metallic Fe clearly emerges (in agreement with the bcc-Fe phase observed by XRD).

2.4. Fenton Reaction. In Fenton-like heterogeneous reactions, catalysis originates from the surface of the catalyst.[36] Hence, the adsorption of H_2O_2 and other reactants at the catalyst surface plays an important role. In the presence of H_2O_2, Fe^0 oxidizes to Fe^{2+} by the transfer of two electrons, as shown in eq 1

$$Fe^0 + H_2O_2 + 2H^+ \rightarrow Fe^{2+} + 2H_2O \quad (1)$$

In the classical Fenton reaction, the production cycle of hydroxyl radicals can be represented as follows[37]

$$Fe^{2+} + H_2O_2 \rightarrow Fe^{3+} + OH^\bullet + OH^- \quad (2)$$

$$Fe^{3+} + H_2O_2 \rightarrow Fe^{2+} + OOH^\bullet + H^+ \quad (3)$$

Furthermore, the ferric ions can be reduced to ferrous ions by the ZVI surface, hence promoting the sustained production cycle of hydroxyl radicals

$$2Fe^{3+} + Fe^0 \rightarrow 3Fe^{2+} \quad (4)$$

In this work, both as-spun and dealloyed nanoporous Fe-rich ribbons show iron oxides and ZVI (the latter in a smaller amount) on the surface. The sustainability of the hydroxyl generation cycle (eqs 1−3) thus depends on the ease of ferrous-ion availability. In this sense, acidity is a crucial parameter for the Fenton oxidation. $OH^\bullet$ radicals cleave azo bonds (−N═N−) in MO previously adsorbed on the catalyst surface, leading to decolorization of the dye solution (Figure 1). The sorption rate can be one of the main controlling factors during the whole catalytic oxidation reaction.[37]

2.4.1. Catalytic Performance of the Ribbons. The catalytic performance of the ribbons was investigated by following the decomposition of MO in an aqueous solution at pH 3 and at a [MO]/[H_2O_2]/[Fe^{2+}] ratio given by[38]

DOI: 10.1021/acsomega.7b00043
ACS Omega 2017, 2, 653−662

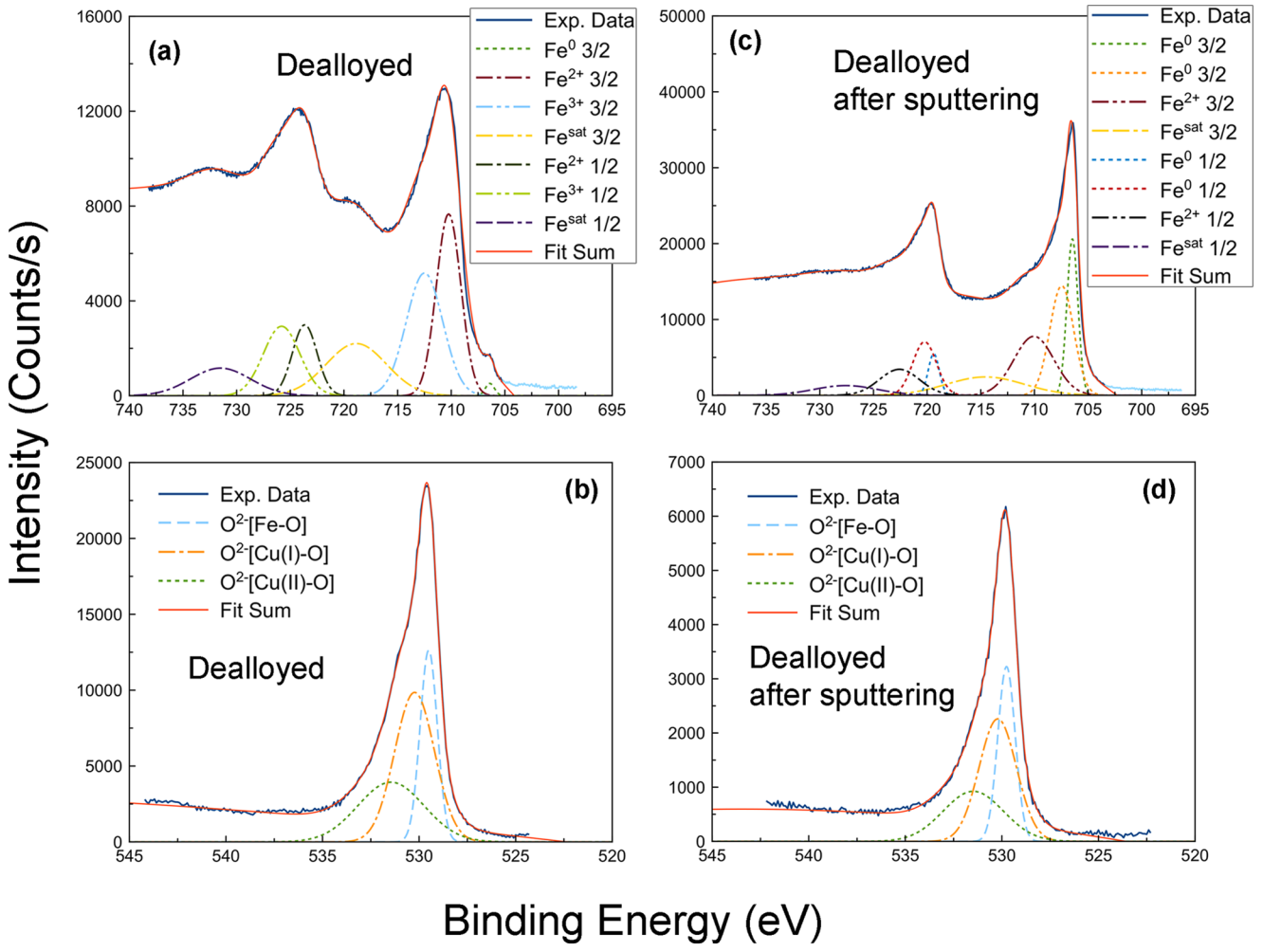

Figure 6. Experimental and deconvoluted high-resolution XPS spectra of (a) Fe 2p and (b) O 1s at the surface level and of (c) Fe 2p and (d) O 1s after 1 min of Ar ions sputtering for the dealloyed ribbon (before the Fenton reaction).

$[MO]:[H_2O_2]:[Fe^{2+}]$ 1:2:0.29

Figure 7a shows the removal efficiency of MO in aqueous solution for both as-spun and dealloyed ribbons, as well as the behavior of a blank solution without catalyst. The results reveal that the dealloyed nanoporous ribbon is much more efficient than the as-spun ribbon in degrading MO. Full degradation of MO occurs in less than 20 min when using the dealloyed ribbon, whereas it takes about 50 min to completely degrade the dye in the presence of the as-spun ribbon. As expected, no significant degradation of MO was observed in the absence of catalyst, which was taken as a reference (blank).

Additionally, inductively coupled plasma (ICP) measurements obtained from the aqueous solution after the Fenton reaction reveal that dissolution of iron from the ribbons occurs during the experiments (see Table 3). Actually, the Fe dissolution is higher in the porous dealloyed sample because 7.58 ppm of Fe is found in this case, whereas only 5.42 ppm of Fe is detected for the as-spun sample after Fenton, which could be explained by the increase in the surface area-to-volume ratio in the nanoporous dealloyed ribbons. The production of ferrous ions accelerates the decomposition of H_2O_2 and the degradation of MO as the Fenton process proceeds, suggesting a combination of heterogeneous and homogeneous degradation reactions when Fe-based alloys are used.[39] To assess the contribution of dissolved iron to the overall degradation process of MO, additional Fenton reactions were performed using $FeSO_4$ as the iron source. Salt dosages were calculated to provide Fe concentrations of 7.58 and 5.42 ppm. As shown in Figure 7b, rapid degradation of MO within the first minute of the assay is observed at both iron concentrations. After this point, reaction rates slow significantly until the complete degradation of MO. This effect might be explained by the Fe^{3+}/Fe^{2+} cycle. Thus, when ferrous iron is used, the initial rate of H_2O_2 decomposition is very rapid. Therefore, the rate of production of $OH^{\bullet}$ and Fe^{3+} is equally rapid (eq 2). However, with the rapid exhaustion of Fe^{2+}, the rate of $OH^{\bullet}$ production also decreases. At this stage, the concentration of ferrous ions depends on the decomposition reaction of Fe^{3+} in presence of H_2O_2 (eq 3), and this reaction is much slower than the former one.

As expected, the experiment at the highest iron concentration gives the fastest degradation rate. However, when comparing the results of the two sets of experiments ($FeSO_4$ and Fe-based ribbons) it was observed that the overall process for complete elimination of MO takes longer for $FeSO_4$ than for their corresponding Fe-based ribbon counterparts. This result indicates that the use of Fe-based alloys is advantageous compared to the use of the conventional $FeSO_4$ reagent. An induction time might be expected to generate surface active iron species.[40] However, in our investigation, we did not

DOI: 10.1021/acsomega.7b00043
ACS Omega 2017, 2, 653−662

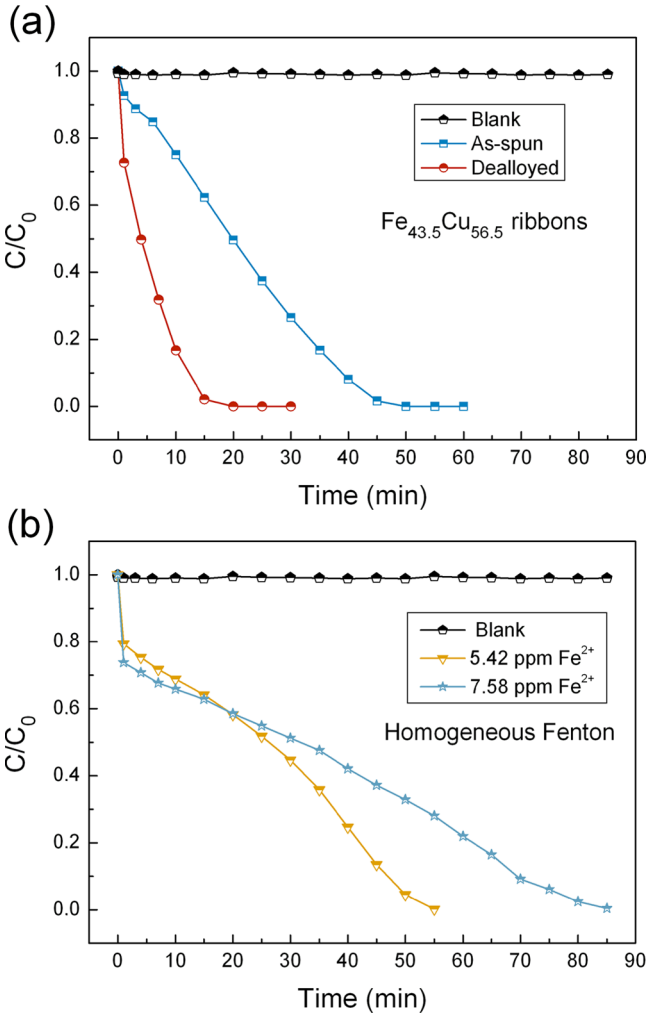

Figure 7. Dependence of the MO concentration as a function of time (i.e., removal efficiency of MO) for the (a) as-spun and dealloyed ribbons and (b) salt solutions (homogeneous Fenton) with the same concentrations of Fe ions as the ones obtained after long-term immersion of the heterogeneous catalysts. All experiments were performed at room temperature for 1 h, at pH 3, and with the addition of 0.1 g L^{-1} H_2O_2 and 50 mg L^{-1} MO.

Table 3. Dissolved Fe and Cu Amounts during the Fenton Reaction Measured by ICP

material	Fe, ppm	Cu, ppm
polished as-spun ribbon	5.42	0.73
dealloyed ribbon	7.58	1.78

observe any induction time for the dealloyed sample, whereas a short induction time could be perceived with the as-spun sample (see Figure 7). In the case of the dealloyed ribbons, this means that the iron species are already available from the very beginning and thus the Fenton reaction takes place immediately.[37] The presence of iron ion species on the surface of the catalyst was actually confirmed by XPS (see Figures 6 and S2).

The enhancement of the catalytic activity of Fe-based alloys might be ascribed to their ability to generate surface hydroxyl radicals and the promotion of Fe^{2+} regeneration at the Fe-based alloy surface (eq 4).[41] Additionally their capacity to continuously release ferrous ions into the solution avoids the rapid consumption of Fe^{2+} and the overload of ferric ions that decreases the degradation rate in the conventional Fenton processes.[42] Actually, in some heterogeneous systems in which the catalytic solid materials serve as a source of metal ions, even submicromolar concentrations of dissolved metal ions contribute to the increase in the degradation rate of the organic contaminant.[43,44] The multiple and complex mechanisms responsible for heterogeneous Fenton reactions have not been fully elucidated yet and remain a topic of extensive investigations.[43] Finally, the higher catalytic activity of the dealloyed ribbons compared to that of the as-spun ones could be assigned to a combination of a higher active surface and iron content. It is believed that the homogeneous Fenton mechanism induced by surface-leached iron and the heterogeneous catalysis mechanism compete differently in the as-cast and porous ribbons.

2.4.2. Structural and Morphological Characterization of the Ribbons after the Fenton Reaction. The XRD patterns of the as-spun and dealloyed ribbons after the Fenton reaction are rather similar to each other, as shown in Figure 8. The main

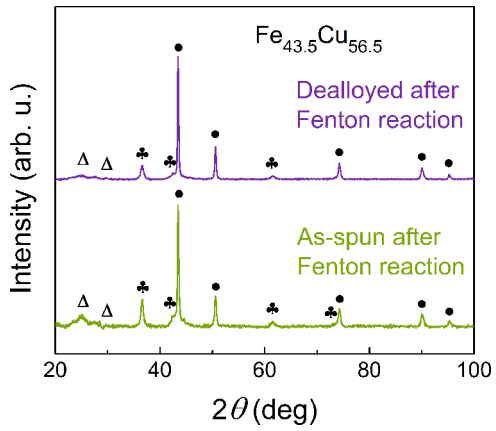

Figure 8. XRD patterns of the as-spun and dealloyed ribbons after the Fenton reaction. The peaks correspond to the fcc-Cu (black filled circle), Cu_2O (black club suit), and η-Fe_2O_3 (open triangle) phases separately.

peaks can be assigned to the fcc-Cu, Cu_2O, and η-Fe_2O_3 (JCPDS Card No. 21-0920) phases. It is thus clear that bcc-Fe tends to dissolve into the solution during the Fenton process, in agreement with ICP analyses (Section 2.4.1). The relative intensity of the η-Fe_2O_3 peaks is slightly higher for the as-spun ribbons, suggesting that dissolution of Fe is more pronounced in the dealloyed ribbon, probably because of its inherent nanoporosity (also in agreement with ICP analyses). The surfaces of the as-spun and dealloyed ribbons after the Fenton reaction are covered by Cu oxides, as confirmed by EDX (Table 1).

In addition, the surface morphology after the Fenton reaction (Figure 9a,c) becomes denser than that before Fenton (Figure 3a,b), particularly in the dealloyed ribbon. The cross-sectional images (Figure 9b,d) show that inside the ribbons the morphology remains similar to that before the Fenton reaction, that is, the dealloyed ribbons exhibit a more obvious nanoporosity. Furthermore, according to EDX, the signal from Fe is very weak after Fenton. A rather low amount of Fe could be detected (2 and 3 atom % for the as-spun and dealloyed ribbons after the Fenton reaction, respectively). Remarkably, in spite of the partial dissolution of the dealloyed

DOI: 10.1021/acsomega.7b00043
ACS Omega 2017, 2, 653−662

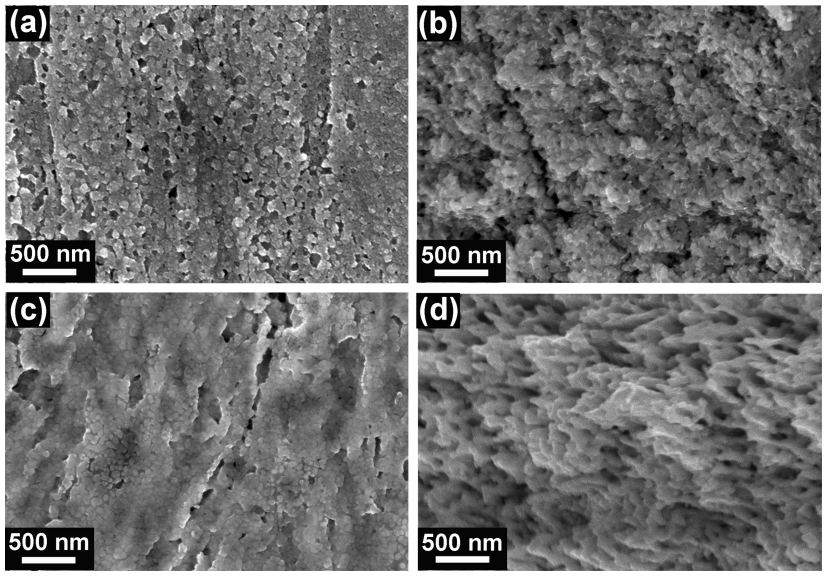

Figure 9. SEM images taken after the Fenton reaction on: (a) the wheel side and (b) the fracture cross-section of the as-spun ribbon and (c) the wheel side and (d) cross-section of the dealloyed ribbon.

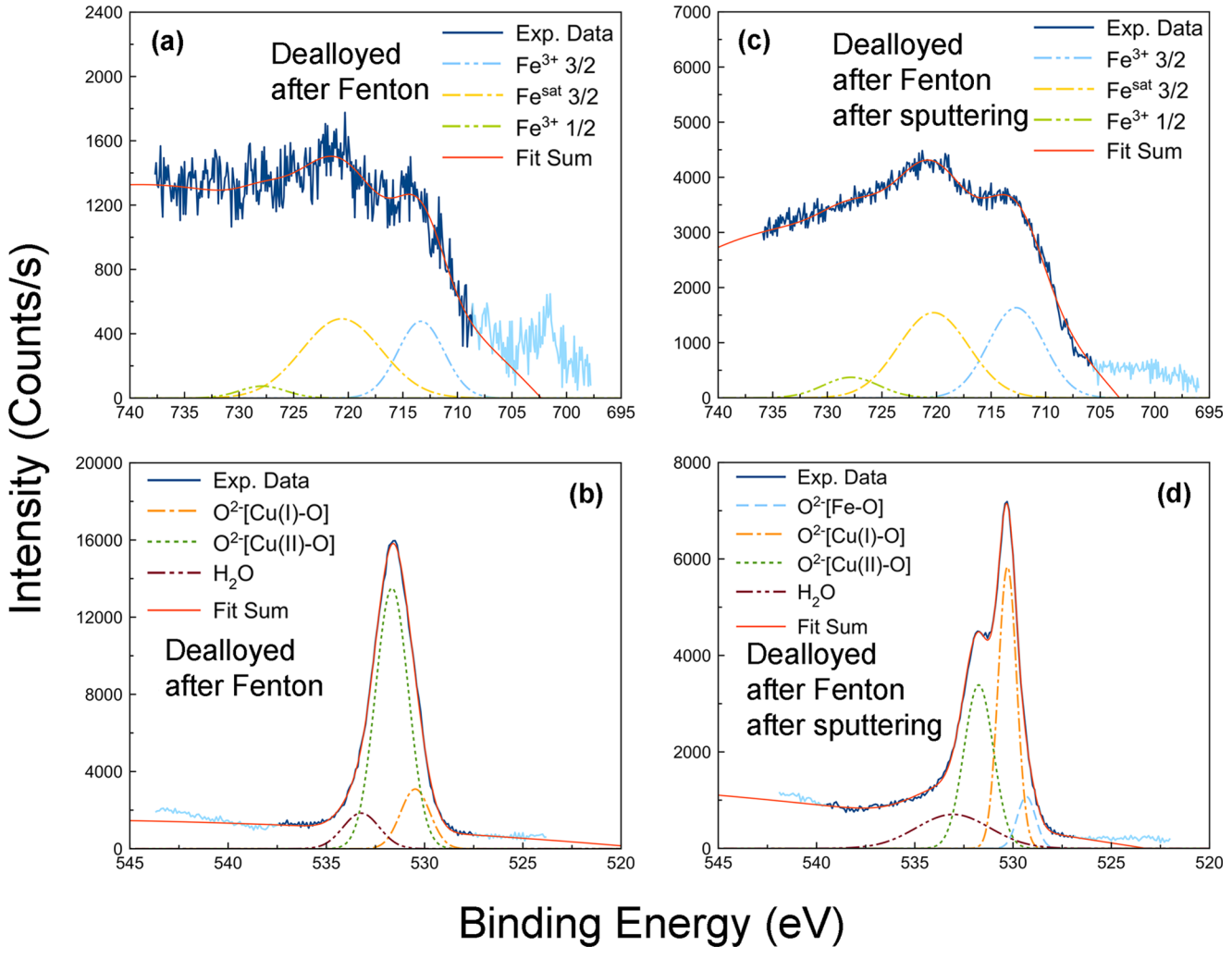

Figure 10. Experimental and deconvoluted high-resolution XPS spectra of (a) Fe 2p and (b) O 1s at the surface level and of (c) Fe 2p and (d) O 1s after 1 min Ar-ion sputtering for the dealloyed ribbon after the Fenton reaction.

DOI: 10.1021/acsomega.7b00043
ACS Omega 2017, 2, 653−662

ribbons during the Fenton reaction, their mechanical integrity was preserved so that the ribbons could be in any case manipulated, even after Fenton studies, for further detailed structural and magnetic characterization. The magnetic hysteresis loops of the samples after the Fenton reaction are displayed in Figure S4, and the corresponding relevant parameters are listed in Table 2. Compared to that of the samples before Fenton, it is obvious that the saturation magnetization of the ribbons after the Fenton reaction decreases significantly. However, clear hysteresis loops with well-defined values of M_r and H_c (inset of Figure S4) indicate there is an obvious ferromagnetic/ferrimagnetic contribution, which probably stems from the η-Fe_2O_3 phase detected by XRD.[45] The lower M_s of the dealloyed ribbon after the Fenton process is probably the consequence of the smaller percentage of the η-Fe_2O_3 phase in this sample as compared to that in the as-spun ribbon after Fenton, as discussed above.

2.4.3. Surface Analysis of the Ribbons after the Fenton Reaction. From the general XPS surface spectra acquired after the Fenton reaction (Figure 5), the intensity of the Fe peaks is found to significantly decrease for both the as-spun and dealloyed ribbons. This result is even more obvious on analyzing the high-resolution Fe 2p region (see Figures S5a and 10a). The deconvoluted contributions indicate the presence of oxidized iron in both cases.

After Ar-ion sputtering, the Fe signal increases but it still remains low. This is in agreement with the remarkable leaching of Fe ions during the Fenton reaction. The core-level Cu 2p (Figure S6) and O 1s (Figures S5b,d and 10b,d) spectra of the two ribbons after the Fenton reaction are very similar, either at the outermost surface or deeper inside the material (i.e., after Ar-ion sputtering). Accordingly, the resulting surfaces after the Fenton reaction are mostly composed of Cu oxides. Interestingly, the Cu(II)/Cu(I) ratio is larger at the surface, indicating that the oxidation degree is higher, as expected from the Fenton reaction.

3. CONCLUSIONS

Fully nanoporous Fe-rich ribbons, with a bcc crystallographic structure and a pore size ranging from 50 to 500 nm, have been obtained by selective dissolution of the fcc-Cu phase from phase-separated $Fe_{43.5}Cu_{56.5}$ ribbons previously prepared by melt-spinning. The nanoporous Fe-rich alloy possesses a higher M_s and slightly higher M_r and H_c than those of the ribbons before dealloying, which can be ascribed to the removal of the paramagnetic Cu-rich phase. The ferromagnetic properties of these ribbons might be used to magnetically guide them toward specific locations in polluted water tanks to degrade organic matter. The dealloyed ribbons exhibited sufficient mechanical integrity during the Fenton reaction processes so that magnetic guiding could indeed be accomplished. Remarkably, the nanoporous dealloyed material is found to be very efficient in degrading MO in an aqueous solution at pH 3, thus acting as an efficient heterogeneous Fenton catalyst. The time needed to fully degrade MO when using the dealloyed ribbon is reduced by roughly a factor 2 as compared to that of the as-spun Fe−Cu ribbons. The efficiency of this catalyst also surpasses that of a homogeneous Fenton reaction when using analogous Fe cation concentrations to those in the aqueous media. The higher catalytic activity of dealloyed ribbons is likely due to its higher surface area and high iron content. Overall, their ability to generate surface hydroxyl radicals, the regeneration of Fe^{2+} at their surfaces, and the sustained release of ferrous ions into the solution avoid the rapid consumption of Fe^{2+} and the overload of ferric ions responsible for the decreased degradation rate in conventional Fenton processes. The combination of highly efficient catalytic activity and convenient production processing makes this nanoporous Fe-rich alloy an interesting candidate material for Fenton catalysis.

4. EXPERIMENTAL PROCEDURES

4.1. Synthesis. Alloy ingots with a nominal composition, $Fe_{43.5}Cu_{56.5}$, were prepared by arc-melting mixtures of high-purity Fe (99.95 wt %) and Cu (99.95 wt %) metals in a Ti-gettered argon atmosphere (the exact alloy composition was determined by EDX, as shown in Table 1). Then, a few pieces of the ingots were remelted and injected into a Cu single roller. Ribbons that were about 1.5 mm wide and 20−25 μm thick were produced by melt-spinning in an argon atmosphere. Subsequently, the ribbons were cut into 30−40 mm long pieces, which were mechanically polished using 4000 grit SiC paper and ultrasonically cleaned in distilled water for 3 min before dealloying. Selective dissolution to obtain the nanoporous ribbon was performed by electrochemical treatment in a 0.065 M HNO_3 solution with an applied voltage of 14 V for 5 min, followed by washing in distilled water (see Figure 1). Both the electrolyte composition and applied voltage were selected on the basis of the electrochemical behavior of the individual elements according to the standard Pourbaix diagrams.[29,46]

4.2. Characterization. Structural characterization of the as-spun and dealloyed samples was carried out by XRD on a Philips X'Pert diffractometer with a pixel one-dimensional detector in the 20−100° 2θ range (step size = 0.026°, total time = 2000 s) using Cu Kα radiation (λ = 0.154178 nm). The surface morphology and fracture cross-section of the ribbons were observed by FESEM (Zeiss Merlin). Hysteresis loops were recorded at room temperature by means of a vibrating sample magnetometer (VSM) from MicroSense. XPS experiments were performed on a PHI 5500 Multitechnique System (from Physical Electronics), with a monochromatic X-ray source (Al Kα line of 1486.6 eV energy and 350 W), under ultrahigh vacuum and a pressure between 5×10^{-9} and 2×10^{-8} torr, placed perpendicular to the analyzer axis and calibrated using the $3d^{5/2}$ line of Ag, with a full width at half-maximum of 0.8 eV. The analyzed area was a circle of 0.8 mm diameter for each sample. The selected resolution for the spectra was 187.85 eV of pass energy and 0.8 eV/step for the general spectra and 23.5 eV of pass energy and 0.1 eV/step for the detailed spectra of the different elements. Composition depth profiles of the dealloyed sample were obtained by sputtering the surface with Ar^+ ions (4 keV energy) for 1 min (about 5−10 nm deep from the sample's surface). Charging effects were corrected by referencing the binding energies to those of the adventitious C 1s line at 284.5 eV. A linear background was assumed.[47] The energy of the deconvoluted peaks was compared to that in the NIST XPS database.[48]

4.3. Fenton Process and Analysis of Samples after the Fenton Reaction. To evaluate the catalytic activity of the iron-based ribbon pieces, MO was used as a model dye. MO is a toxic azo dye usually found in textile wastewater that causes a severe ecological impact. All chemicals for the Fenton reaction (i.e., MO, hydrogen peroxide, sodium sulfate, and sulfuric acid) were supplied by Scharlau and used without further purification. To compare the catalytic efficiency of the ribbons before and after dealloying, MO solutions with an initial concentration of 50 mg L^{-1} were prepared by diluting 1 g L^{-1}

DOI: 10.1021/acsomega.7b00043
ACS Omega 2017, 2, 653−662

stock solutions in deionized water. To carry out the experiments, 1.51 mg of the as-spun ribbon and 1.42 mg of the dealloyed ribbon were introduced, separately, into a 100 mL MO solution. Then, 710 mg of Na_2SO_4 (final concentration 50 mM) was added to simulate natural wastewater pollutants and the pH was adjusted to 3 using H_2SO_4 (because the reported optimum pH is between 2 and 3 for the Fenton reaction catalyzed by ZVI).[49,50] Separately, a 0.1 g L^{-1} H_2O_2 solution was also prepared. The reaction was started by adding this H_2O_2 solution. The solution mixture was continuously stirred, and the reaction was performed at room temperature for 1 h or until complete degradation of MO was achieved. Aliquots were withdrawn every 5 or 10 min from the reaction beaker, and the concentration of MO was measured using a Jasco V-570 UV spectrophotometer at a wavelength of 505 nm, which corresponded to the maximum absorption of the solution at the beginning of the experiment (pH 3). After that, the aliquot was poured back into the beaker. Additionally, a blank experiment was performed, in which no ribbon catalyst was added.

The structure, morphology, and magnetic properties of the ribbons after the Fenton reaction were investigated by XRD, FESEM-EDX, and VSM. The concentrations of the metallic cations leached into the solution after the Fenton experiments were measured by ICP spectroscopy (ICPE 9000, Shimadzu). For this purpose, 17 and 13 mL of the solution were extracted from the reaction vessels containing the as-spun and dealloyed ribbons, respectively. XPS experiments, including compositional depth measurements, were performed using the same equipment, parameters, and analysis methodology as those mentioned above. To carry out comparative homogeneous Fenton reactions, the same procedure was applied using $FeSO_4 \cdot 7H_2O$ instead of Fe-based ribbons. Salt dosages were chosen to coincide with those measured by ICP at the end of the previous experiments.

■ ASSOCIATED CONTENT

Supporting Information

The Supporting Information is available free of charge on the ACS Publications website at DOI: 10.1021/acsomega.7b00043.

Additional details and figures as mentioned in the text (PDF)

■ AUTHOR INFORMATION

Corresponding Authors

*E-mail: eva.pellicer@uab.cat (E.P.).
*E-mail: jordi.sort@uab.cat (J.S.).

ORCID

Jordi Sort: 0000-0003-1213-3639

Author Contributions

The manuscript was written through contributions from all authors. H.Z., E.P., and J.S. conceived and designed this work. H.Z. and Y.F. executed the dealloying process and characterization measurements. The original ribbon samples were prepared and provided by Y.C. and T.Z. A.A., E.G.-L., and F.A. performed the Fenton reaction. H.Z. wrote the draft. E.P., J.S., M.D.B., E.G.-L., and F.A. reviewed and edited the draft. All authors have given approval to the final version of the manuscript.

Notes

The authors declare no competing financial interest.

■ ACKNOWLEDGMENTS

This work was partially funded by the Generalitat de Catalunya (2014-SGR-1015) and the Spanish Ministerio de Economía y Competitividad (MAT2014-57960-C3-1-R, cofinanced by the Fondo Europeo de Desarrollo Regional, FEDER, MAT2014-57960-C3-2-R, and CTQ2013-48897-C2-2-R). Y.F. is grateful for his CSC Grant. Dr. E.P. is grateful to MINECO for the "Ramon y Cajal" contract (RYC-2012-10839).

■ REFERENCES

(1) Ikehata, K.; El-din, M. G. M. Aqueous Pesticide Degradation by Hydrogen Peroxide/Ultraviolet Irradiation and Fenton-Type Advanced Oxidation Processes: A Review. *J. Environ. Eng. Sci.* **2006**, *5*, 81−135.

(2) Georgi, A.; Kopinke, F. D. Interaction of Adsorption and Catalytic Reactions in Water Decontamination Processes: Part I. Oxidation of Organic Contaminants with Hydrogen Peroxide Catalyzed by Activated Carbon. *Appl. Catal., B* **2005**, *58*, 9−18.

(3) Yoshida, Y.; Ogata, S.; Nakamatsu, S.; Shimamune, T.; Kikawa, K.; Inoue, H.; Iwakura, C. Decoloration of Azo Dye Using Atomic Hydrogen Permeating Through a Pt-Modified Palladized Pd Sheet Electrode. *Electrochim. Acta* **1999**, *45*, 409−414.

(4) Dutta, K.; Mukhopadhyay, S.; Bhattacharjee, S.; Chaudhuri, B. Chemical Oxidation of Methylene Blue Using a Fenton-Like Reaction. *J. Hazard. Mater.* **2001**, *84*, 57−71.

(5) Gogate, P. R.; Pandit, A. B. A Review of Imperative Technologies for Wastewater Treatment I: Oxidation Technologies at Ambient Conditions. *Adv. Environ. Res.* **2004**, *8*, 501−551.

(6) Casero, I.; Sicilia, D.; Rubio, S.; Perez-Bendito, D. Chemical Degradation of Aromatic Amines by Fenton's Reagent. *Water Res.* **1997**, *31*, 1985−1995.

(7) Kuo, W. G. Decolorizing Dye Wastewater with Fenton's Reagent. *Water Res.* **1992**, *26*, 881−886.

(8) Nam, S.; Renganathan, V.; Tratnyek, P. G. Substituent Effects on Azo Dye Oxidation by the Fe III−EDTA−H_2O_2 System. *Chemosphere* **2001**, *45*, 59−65.

(9) Barbusiński, K. The Modified Fenton Process for Decolorizationof Dye Wastewater. *Pol. J. Environ. Stud.* **2005**, *14*, 281−285.

(10) Huston, P. L.; Pignatello, J. J. Degradation of Selected Pesticide Active Ingredients and Commercial Formulations in Water by the Photo-Assisted Fenton Reaction. *Water Res.* **1999**, *33*, 1238−1246.

(11) Lin, S. H.; Lin, C. M.; Leu, H. G. Operating Characteristics and Kinetic Studies of Surfactant Wastewater Treatment by Fenton Oxidation. *Water Res.* **1999**, *33*, 1735−1741.

(12) Liou, M. J.; Lu, M. C.; Chen, J. N. Oxidation of Explosives by Fenton and Photo-Fenton Processes. *Water Res.* **2003**, *37*, 3172−3179.

(13) Brillas, E.; Sirés, I.; Oturan, M. A. Electro-Fenton Process and Related Electrochemical Technologies Based on Fenton's Reaction Chemistry. *Chem. Rev.* **2009**, *109*, 6570−6631.

(14) Arnold, S. M.; Hickey, W. J.; Harris, R. F. Degradation of Atrazine by Fenton's Reagent: Condition Optimization and Product Quantification. *Environ. Sci. Technol.* **1995**, *29*, 2083−2089.

(15) Zazo, J. A.; Casas, J. A.; Mohedano, A. F.; Rodríguez, J. J. Catalytic Wet Peroxide Oxidation of Phenol with a Fe/Active Carbon Catalyst. *Appl. Catal., B* **2006**, *65*, 261−268.

(16) Sharma, V. K. Ferrate (VI) and Ferrate (V) Oxidation of Organic Compounds: Kinetics and Mechanism. *Coord. Chem. Rev.* **2013**, *257*, 495−510.

(17) Hartmann, M.; Kullmann, S.; Keller, H. Wastewater Treatment with Heterogeneous Fenton-Type Catalysts Based on Porous Materials. *J. Mater. Chem.* **2010**, *20*, 9002−9017.

(18) Xu, H. Y.; Qi, S. Y.; Li, Y.; Zhao, Y.; Li, J. W. Heterogeneous Fenton-Like Discoloration of Rhodamine B Using Natural Schorl as Catalyst: Optimization by Response Surface Methodology. *Environ. Sci. Pollut. Res.* **2013**, *20*, 5764−5772.

(19) Karthikeyan, S.; Titus, A.; Gnanamani, A.; Mandal, A. B.; Sekaran, G. Treatment of Textile Wastewater by Homogeneous and

DOI: 10.1021/acsomega.7b00043
ACS Omega 2017, 2, 653−662

Heterogeneous Fenton Oxidation Processes. *Desalination* **2011**, *281*, 438−445.
(20) Fontecha-Cámara, M. A.; Álvarez-Merino, M. A.; Carrasco-Marín, F.; López-Ramón, M. V.; Moreno-Castilla, C. Heterogeneous and Homogeneous Fenton Processes Using Activated Carbon for the Removal of the Herbicide Amitrole from Water. *Appl. Catal., B* **2011**, *101*, 425−430.
(21) Calleja, G.; Melero, J. A.; Martínez, F.; Molina, R. Activity and Resistance of Iron-Containing Amorphous, Zeolitic and Mesostructured Materials for Wet Peroxide Oxidation Of Phenol. *Water Res.* **2005**, *39*, 1741−1750.
(22) Rusevova, K.; Kopinke, F. D.; Georgi, A. Nano-Sized Magnetic Iron Oxides as Catalysts for Heterogeneous Fenton-Like Reactions—Influence of Fe (II)/Fe (III) Ratio on Catalytic Performance. *J. Hazard. Mater.* **2012**, *241*−*242*, 433−440.
(23) Babuponnusami, A.; Muthukumar, K. Removal of Phenol by Heterogenous Photo Electro Fenton-Like Process Using Nano-Zero Valent Iron. *Sep. Purif. Technol.* **2012**, *98*, 130−135.
(24) Wang, Y.; Zhao, H.; Zhao, G. Iron-Copper Bimetallic Nanoparticles Embedded within Ordered Mesoporous Carbon as Effective and Stable Heterogeneous Fenton Catalyst for the Degradation of Organic Contaminants. *Appl. Catal., B* **2015**, *164*, 396−406.
(25) Luo, L.; Dai, C.; Zhang, A.; Wang, J.; Liu, M.; Song, C.; Guo, X. A Facile Strategy for Enhancing FeCu Bimetallic Promotion for Catalytic Phenol Oxidation. *Catal. Sci. Technol.* **2015**, *5*, 3159−3165.
(26) Wang, J.; Liu, C.; Tong, L.; Li, J.; Luo, R.; Qi, J.; Li, Y.; Wang, L. Iron−Copper Bimetallic Nanoparticles Supported on Hollow Mesoporous Silica Spheres: An Effective Heterogeneous Fenton Catalyst for Orange II Degradation. *RSC Adv.* **2015**, *5*, 69593−69605.
(27) Parmar, J.; Vilela, D.; Pellicer, E.; Esqué-de los Ojos, D.; Sort, J.; Sánchez, S. Reusable and Long-Lasting Active Microcleaners for Heterogeneous Water Remediation. *Adv. Funct. Mater.* **2016**, *26*, 4152−4161.
(28) McCue, I.; Benn, E.; Gaskey, B.; Erlebacher, J. Dealloying and Dealloyed Materials. *Annu. Rev. Mater. Res.* **2016**, *46*, 263−286.
(29) Park, B. J.; Chen, Y. M.; Ohkubo, T. Metallic Porous Materials' Design with Phase Separation in Fe−Cu And Co−Cu Systems. *Intermetallics* **2009**, *17*, 958−961.
(30) Niyomsoan, S.; Gargarella, P.; Chomsaeng, N.; Termsuksawad, P.; Kühn, U.; Eckert, J. Phase Separation in Rapid Solidified Ag-Rich Ag-Cu-Zr Alloys. *Mater. Res.* **2015**, *18*, 120−126.
(31) Kuncser, V.; Valeanu, M.; Lifei, F.; Predoi, D.; Jianu, A.; Kappel, W.; Codescu, M.; Patroi, E.; Pasuk, I.; Bulinski, M.; Filoti, G. Micro-Structure and Magnetic Properties of Fe−Cu Nanocomposites for Anisotropic Permanent Magnets. *J. Alloys Compd.* **2005**, *395*, 1−6.
(32) Lee, D. W.; Ryan, D. H.; Altounian, Z.; Kuprin, A. Structural and Magnetic Properties of Cu/Fe Multilayers. *Phys. Rev. B* **1999**, *59*, 7001−7009.
(33) Cullity, B. D.; Graham, C. D. *Introduction to Magnetic Materials*; Wiley-IEEE Press: Piscataway, 2009.
(34) Sato, F.; Tezuka, N.; Sakurai, T.; Miyazaki, T. Grain Diameter and Coercivity of Fe, Ni, and Co Metals. *IEEE Transl. J. Magn. Jpn.* **1994**, *9*, 100−106.
(35) Li, X.; Cao, J.; Zhang, W. Stoichiometry of Cr(VI) Immobilization Using Nanoscale Zerovalent Iron (Nzvi): A Study with High-Resolution X-Ray Photoelectron Spectroscopy (HR-XPS). *Ind. Eng. Chem. Res.* **2008**, *47*, 2131−2139.
(36) Wang, N.; Zheng, T.; Zhang, G.; Wang, P. A Review on Fenton-Like Processes for Organic Wastewater Treatment. *J. Environ. Chem. Eng.* **2016**, *4*, 762−787.
(37) Shahwan, T.; Sirriah, S. A.; Nairat, M.; Boyaci, E.; Eroğlu, A. E.; Scott, T. B.; Hallam, K. R. Green Synthesis of Iron Nanoparticles and Their Application as a Fenton-Like Catalyst for the Degradation of Aqueous Cationic and Anionic Dyes. *Chem. Eng. J.* **2011**, *172*, 258−266.
(38) García-Rojas, O.; Gómez-Quintero, C.; Ríos-Bolívar, M.; Romero, A.; Rodríguez, A. In *Study and Modeling of Methylorange Degradation with the Fenton Reaction*, Proceedings of the 9th WSEAS International Conference on Computational Intelligence, Man-Machine Systems and Cybernetics, 2010; pp 251−258.
(39) Zhou, T.; Li, Y.; Li, J.; Wong, F.-S.; Lu, X. Oxidation of 4-Chlorophenol in a Heterogeneous Zero Valent Iron/H_2O_2 Fenton-Like System: Kinetic, Pathway and Effect Factors. *Sep. Purif. Technol.* **2008**, *62*, 551−558.
(40) Hassan, H.; Hameed, B. H. In *Decolorization of Acid Red 1 by Heterogeneous Fenton-Like Reaction Using Fe-Ball Clay Catalyst*, International Conference on Environment Science and Engineering, IPCBEE, 2011; pp 232−236.
(41) Xiang, W.; Zhang, B.; Zhou, T.; Wu, X.; Mao, J. An Insight in Magnetic Field Enhanced Zero-Valent Iron/H_2O_2 Fenton-Like Systems: Critical Role and Evolution of the Pristine Iron Oxides Layer. *Sci. Rep.* **2016**, *6*, No. 24094.
(42) Carra, I.; Malato, S.; Jiménez, M.; Maldonado, M. I.; Sánchez Pérez, J. A. Microcontaminant Removal by Solar Photo-Fenton at Natural pH Run with Sequential and Continuous Iron Additions. *Chem. Eng. J.* **2014**, *235*, 132−140.
(43) He, J.; Yang, X.; Men, B.; Wang, D. Interfacial mechanisms of heterogeneous Fenton reactions catalyzed by iron-based materials: A review. *J. Environ. Sci.* **2016**, *39*, 97−109.
(44) Kuan, C.-C.; Chang, S.-Y.; Schroeder, S. L. M. Fenton-Like Oxidation of 4-Chlorophenol: Homogeneous or Heterogeneous? *Ind. Eng. Chem. Res.* **2015**, *54*, 8122−8129.
(45) Zhong, J.; Cao, C.; Liu, H.; Ding, Y.; Yang, J. Fabrication of Hollow and Yolk−Shell Structured η-Fe_2O_3 Nanoparticles with Versatile Configurations. *Ind. Eng. Chem. Res.* **2013**, *52*, 1303−1308.
(46) Parsons, R. Atlas of Electrochemical Equilibria in Aqueous Solutions. *J. Electroanal. Chem. Interfacial Electrochem.* **1967**, *13*, 471.
(47) Repoux, M. Comparison of Background Removal Methods for XPS. *Surf. Interface Anal.* **1992**, *18*, 567−570.
(48) NIST X-ray Photoelectron Spectroscopy Database, version 4.1, 2012. http//:srdata.nist.gov/xps/.
(49) Hsueh, C. L.; Huang, Y. H.; Wang, C. C.; Chen, C. Y. Degradation of Azo Dyes Using Low Iron Concentration of Fenton and Fenton-Like System. *Chemosphere* **2005**, *58*, 1409−1414.
(50) Devi, L. G.; Kumar, S. G.; Reddy, K. M.; Munikrishnappa, C. Photo Degradation of Methyl Orange an Azo Dye by Advanced Fenton Process Using Zero Valent Metallic Iron: Influence of Various Reaction Parameters and Its Degradation Mechanism. *J. Hazard. Mater.* **2009**, *164*, 459−467.

DOI: 10.1021/acsomega.7b00043
ACS Omega 2017, 2, 653−662